

OpenDPDv2: A Unified Learning and Optimization Framework for Neural Network Digital Predistortion

Yizhuo Wu[✉], Graduate Student Member, Ang Li[✉], Graduate Student Member, Chang Gao^{*✉}, Member

Abstract—Neural network (NN)-based Digital Predistortion (DPD) stands out in improving signal quality in wideband radio frequency (RF) power amplifiers (PAs) employing complex modulation. However, NN DPDs usually rely on a large number of parameters for effective linearization and can significantly contribute to the energy consumption of the digital back-end in RF systems. This paper presents OpenDPDv2, a unified framework for PA modeling, DPD learning, and model optimization to reduce power consumption while maintaining high linearization performance. The optimization techniques feature a novel DPD algorithm, TRes-DeltaGRU, alongside two energy-efficient methods. The top-performing 32-bit floating-point (FP32) TRes-DeltaGRU-DPD model achieves an Adjacent Channel Power Ratio (ACPR) of -59.4 dBc and Error Vector Magnitude (EVM) of -42.1 dBc. By exploiting fixed-point quantization and dynamic temporal sparsity of input signals and hidden neurons, the inference energy of our model can be reduced by 4.5 \times while still maintaining -50.3 dBc Adjacent Channel Power Ratio (ACPR) and -35.2 dB in Error Vector Magnitude (EVM) with 56% temporal sparsity evaluated with a TM3.1a 200MHz-BW 256-QAM OFDM signal applied to a 3.5 GHz GaN Doherty RF PA. OpenDPDv2 code, datasets, and documentation are publicly accessible at <https://github.com/lab-emi/OpenDPD>.

Index Terms—digital predistortion (DPD), temporal sparsity, power amplifier (PA), recurrent neural network (RNN), digital signal processing (DSP)

I. INTRODUCTION

THE exponential growth of wireless data traffic has driven growing demands for broader spectrum usage, higher data rates and fewer error occurrences in modern wireless communication systems. However, wideband Radio Frequency (RF) Power Amplifiers (PAs), as an essential component in TX systems, degrade the signal quality by inherent distortions. These distortions raise out-of-band emissions power and in-band symbol errors, which negatively affect both the reliability of communications and energy efficiency. To address these challenges, Digital Pre-distortion (DPD) has become a promising method.

DPD aims to derive an inverse function of PAs transfer function to compensate for nonlinearity before the signal passes through the RF transmitter. Conventional DPD methods based on Volterra-series deliver effective linearization in narrowband scenarios but struggle with wideband and high-constellation modulated signals to satisfy communication standards [1]. In contrast, Machine Learning (ML) techniques, such as Neural Network (NN)-based DPD, outperform Generalized Memory Polynomial (GMP) model

for Orthogonal Frequency Division Modulation (OFDM) signal with bandwidth higher than 200 MHz and meet the requirement of communication standard [2]–[5].

However, the DPD module consumes a substantial portion of power in wideband radio digital back-ends [6]. The incorporation of Neural Networks (NNs) could further intensify this power issue. The power usage in digital signal processors, contrary to the purpose of the efficient implementation for wideband transmitters in basestations and Wi-Fi routers, where power resources are constrained.

Previous approaches to reduce DPD energy consumption include lowering the sample rate [7], employing a sub-Nyquist feedback receiver in the observation path [8], dynamically adjusting model cross-terms based on input signal characteristics [9], simplifying computational pathways for DPD algorithms [10], and pruning less critical weights in fully connected layers to achieve static spatial weight sparsity [11].

This article presents OpenDPDv2, a unified open-source NN-based DPD framework for accurate PA modeling, DPD learning, and in-situ model optimization towards reduced arithmetic operations and energy-expensive memory accesses, and goes beyond our previous works [12]–[15]. OpenDPDv2 incorporates a new high-performance hybrid-NN-based DPD algorithm with high linearization performance and optimized energy efficiency through dynamic temporal sparsity and quantization-aware training. The main contributions are:

- 1) We present OpenDPDv2, an open-source, end-to-end (E2E) learning framework crafted in PyTorch [16] to enable fast prototyping of accurate and power-efficient NN-based DPD algorithms by streamlining learning and optimization through DPD quantization and temporal sparsity exploitation.
- 2) OpenDPDv2 comes with a new TM3.1a (256 QAM-OFDM) 5-channel \times 40 MHz (200 MHz) test signal dataset, measured from a 3.5 GHz Ampleon GaN Power Amplifier (PA) @ 41.5 dBm average output power, named APA_200MHz, for free access of the community to precise PA measurement data for modeling, DPD learning and potential development of other digital signal processing algorithms and systems.
- 3) OpenDPDv2 embeds a new temporal residual (TRes)-DeltaGRU NN DPD algorithm, achieving decent measured linearization performance at -59.4 dBc ACPR with 1000 32-bit floating-point (FP) parameters.
- 4) We provide energy estimation results derived from a simulated ARM CPU platform using Gem5, a widely-adopted open-source computer architecture

*Corresponding author: Chang Gao (chang.gao@tudelft.nl)

Yizhuo Wu, Ang Li, and Chang Gao are with the Department of Microelectronics, Delft University of Technology, The Netherlands.

simulator, providing accurate statistics of committed instructions and memory access patterns of a practical processor. OpenDPDv2 managed to reduce $4.5\times$ the inference energy consumption of a 1000-parameter TRes-DeltaGRU DPD model while still maintain -50.3 dBc ACPR and -35.2 dB EVM for the TM3.1a 200MHz test signal.

II. NN-BASED DPD'S POWER ISSUE

A. Overview

This section provides a comprehensive analysis of power consumption in NN-based DPD systems to prepare for later discussions and identifies pathways toward energy-efficient implementations suitable for mass deployment.

Figure 1 (a) illustrates the operational cycle of a practical DPD system, where periodic IQ data collection and model parameter updates (adaptation) interleave with continuous DPD inference. This cyclic operation reveals that the total power consumption of an NN-based DPD engine, P_{DPD} , can be decomposed into three principal components:

$$\begin{aligned} P_{\text{DPD}} &= P_{\text{INF}} + P_{\text{SAM}} + P_{\text{ADA}} \\ &= \frac{E_{\text{INF}}}{T_{\text{DPD}}} + \frac{E_{\text{SAM}}}{T_{\text{DPD}}} + \frac{E_{\text{ADA}}}{T_{\text{DPD}}} \end{aligned} \quad (1)$$

where:

- T_{DPD} : cyclic period of DPD operation, spanning between the starting point of data sample collections from the Transmitter Observation Receiver (TOR) [17] in neighboring DPD operation cycles, which includes high-speed Analog-to-Digital Converters (ADC), down-conversion, and associated processing for online adaptation.
- E_{INF} : energy consumed during DPD inference (INF), encompassing per-sample forward pass of the NN DPD model throughout T_{DPD} .
- E_{SAM} : energy drawn by the TOR during IQ data sample collection (SAM) collection.
- E_{ADA} : energy expended in updating the DPD model parameters for online adaptation (ADA).

B. Inference Power (P_{INF}): The Dominant Factor

In a streaming transmitter, DPD inference operates continuously throughout T_{DPD} , processing each incoming I/Q sample at the sampling rate f_s . The inference energy consumption is fundamentally tied to the computational complexity of the NN model:

$$E_{\text{INF}} = E_F \cdot N_F = E_F \cdot f_s \cdot T_{\text{DPD}}, \quad (2)$$

where:

- E_F : energy per forward pass, encompassing arithmetic operations (multiplications, additions, nonlinear activations) and memory accesses.
- N_F : total number of forward passes during T_{DPD} .

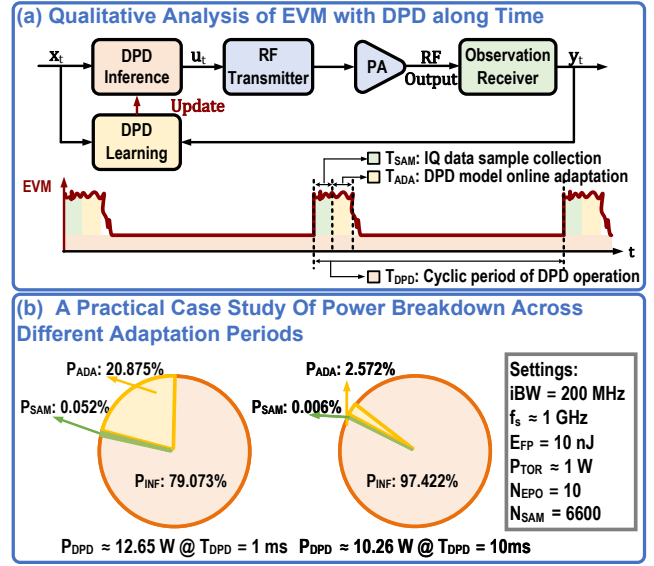


Fig. 1. (a) Qualitative Analysis of EVM with DPD vs. Time. (b) A practical case study of power breakdown across different adaptation periods.

Consequently, the DPD inference power consumption becomes:

$$P_{\text{INF}} = \frac{E_{\text{INF}}}{T_{\text{DPD}}} = E_F \cdot f_s \quad (3)$$

As wireless systems push toward multi-GHz sampling rates for wider bandwidths, inference power will scale proportionally and potentially reach prohibitive levels.

C. Data Collection Power (P_{SAM}): The Periodic Overhead

Maintaining accurate linearization requires periodic acquisition of high-quality I/Q samples from the TOR. The power contribution from this sampling process is:

$$\begin{aligned} P_{\text{SAM}} &= \frac{P_{\text{TOR}} \cdot T_{\text{SAM}}}{T_{\text{DPD}}} \\ &\approx \frac{P_{\text{ADC}} \cdot N_{\text{SAM}}}{T_{\text{DPD}} \cdot f_s}, \end{aligned} \quad (4)$$

where P_{TOR} represents the TOR's active power consumption approximating the ADC power, which is the dominant part. $T_{\text{SAM}} = N_{\text{SAM}}/f_s$ denotes the data acquisition duration (as shown in Fig. 1 (a)), and N_{SAM} is the number of collected I/Q samples.

Notably, this component exhibits an inverse relationship with the adaptation period T_{DPD} , allowing system designers to trade off adaptation frequency against power consumption based on PA characteristics.

D. Adaptation Power (P_{ADA}): The Online Learning Cost

While most existing NN-based DPD studies focus on offline implementations, practical deployments must address long-term PA variations, including thermal drift, electron trapping, and bias-point shifts that evolve over microseconds to milliseconds [18]. Online adaptation via backpropagation [19] incurs significant computational overhead, with each epoch

requiring both forward (F) passes and backward (B) passes. Given that each backward pass typically requires $2\text{--}3\times$ the computational resources of a forward pass, the adaptation power consumption can be estimated as:

$$P_{\text{ADA}} = \frac{(E_F + E_B) \cdot N_{\text{EPO}} \cdot N_{\text{SAM}}}{T_{\text{DPD}}} \approx \frac{4E_F \cdot N_{\text{EPO}} \cdot N_{\text{SAM}}}{T_{\text{DPD}}} \quad (5)$$

where E_B is the energy per backward pass and N_{EPO} is the number of online adaptation epochs.

E. DPD Power Breakdown: A Practical Case Study

Synthesizing Eqs. 1, 2, 4, and 5, the total DPD power consumption becomes:

$$P_{\text{DPD}} = E_F \cdot f_s + \frac{P_{\text{ADC}} \cdot N_{\text{SAM}}}{T_{\text{DPD}} \cdot f_s} + \frac{4E_F \cdot N_{\text{EPO}} \cdot N_{\text{SAM}}}{T_{\text{DPD}}} \quad (6)$$

To ground this analysis in practical numbers, consider a TM3.1a test signal with 200 MHz baseband bandwidth sampled at 983.04 MHz (approximated to 1 GHz for clarity). Below are the assumptions:

- **Forward pass energy:** $E_F = 10\text{ nJ}$ per forward pass for a 1000-parameter Gated Recurrent Unit (GRU)-based DPD [14];
- **Data collection:** assuming $P_{\text{ADC}} \approx 1\text{ W}$ for 12-bit precision at 1 GHz sample rate [20];
- **Adaptation parameters:** $N_{\text{EPO}} = 10$ epochs, $N_{\text{SAM}} = 6600$ samples (normalized from 2000 samples at 300 MHz [21]);
- **Update period:** T_{DPD} ranging from 1 ms to 1 s;

Figure 1 (b) presents the power breakdown across different adaptation periods. For $T_{\text{DPD}} = 1\text{ ms}$, the total power consumption reaches:

$$P_{\text{DPD}} = P_{\text{INF}} + P_{\text{SAM}} + P_{\text{ADA}} = 10.0 + 0.0066 + 2.64 = 12.65 \text{ (W)}$$

This analysis reveals a critical insight: inference power dominates the total consumption ($>79\%$), even with aggressive adaptation rates. For $T_{\text{DPD}} = 10\text{ ms}$, the total power consumption is approximately 10.26 W. As T_{DPD} increases toward more practical values (e.g., 1 s), the inference component exceeds 99% of total power, while adaptation and sampling contributions become negligible. The reason this P_{DPD} is way higher than common DPD power numbers showing up in industrial product datasheets is because here we assume a completely real-time streaming large complex NN DPD @ 1 GHz sample rate under 100% duty cycle, which does not exist in any physical product yet.

F. Implications for Power-Efficient Wideband DPD Design

As the inference power dominates and scales linearly with model complexity and sampling rate, the primary path towards energy-efficient NN DPD lies in aggressively reducing E_F through model compression, such as quantization [13] and model sparsification methods [11], [14], [22], dedicated

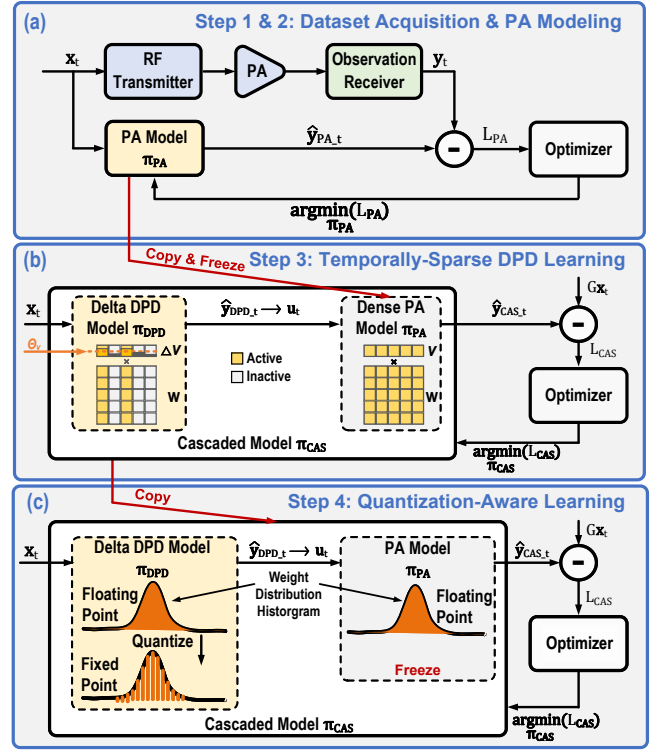


Fig. 2. Learning and optimization flow of OpenDPDv2.

hardware accelerators on FPGAs [23] or even in ASICs [24], and low-sampling-rate DPD [7] or sub-Nyquist TOR techniques [25].

Therefore, in this work, we integrate the DPD learning and optimization through model quantization and temporally sparsification to reduce DPD forward pass complexity, which contributes to the reduction of P_{INF} and P_{ADA} .

III. OPENDPDv2

OpenDPDv2 extends OpenDPDv1 [12] with the new Temporal Residual Delta Gated Recurrent Unit (TRes-DeltaGRU) algorithm and two optimization methodologies, including temporal sparsity through delta threshold mechanisms and quantization-aware training for hardware-efficient deployment. As depicted in Fig. 2, the architecture of OpenDPDv2 comprises four primary steps. Steps 1 and 2 maintain the foundational framework of OpenDPDv1, while steps 3 and 4 introduce the temporal sparse DPD learning and quantization-aware learning methodologies:

- 1) **Data Acquisition & PA Modeling (Fig. 2a):** The baseband input I/Q signal is represented as $\mathbf{X} = \{\mathbf{x}_t | \mathbf{x}_t = I_{\mathbf{x}_t} + jQ_{\mathbf{x}_t}, I_{\mathbf{x}_t}, Q_{\mathbf{x}_t} \in \mathbb{R}, t \in 0, \dots, T-1\}$. Transmitting it through the PA, the baseband output signals are captured as $\mathbf{Y} = \{\mathbf{y}_t | \mathbf{y}_t = I_{\mathbf{y}_t} + jQ_{\mathbf{y}_t}, I_{\mathbf{y}_t}, Q_{\mathbf{y}_t} \in \mathbb{R}, t \in 0, \dots, T-1\}$. A behavioral PA model, π_{PA} , is trained via BackPropagation Through Time (BPTT) to minimize the Mean Square Error (MSE) between predicted $\hat{\mathbf{y}}_{\text{PA}}[n]$ and ground truth PA output $\mathbf{y}[n]$.

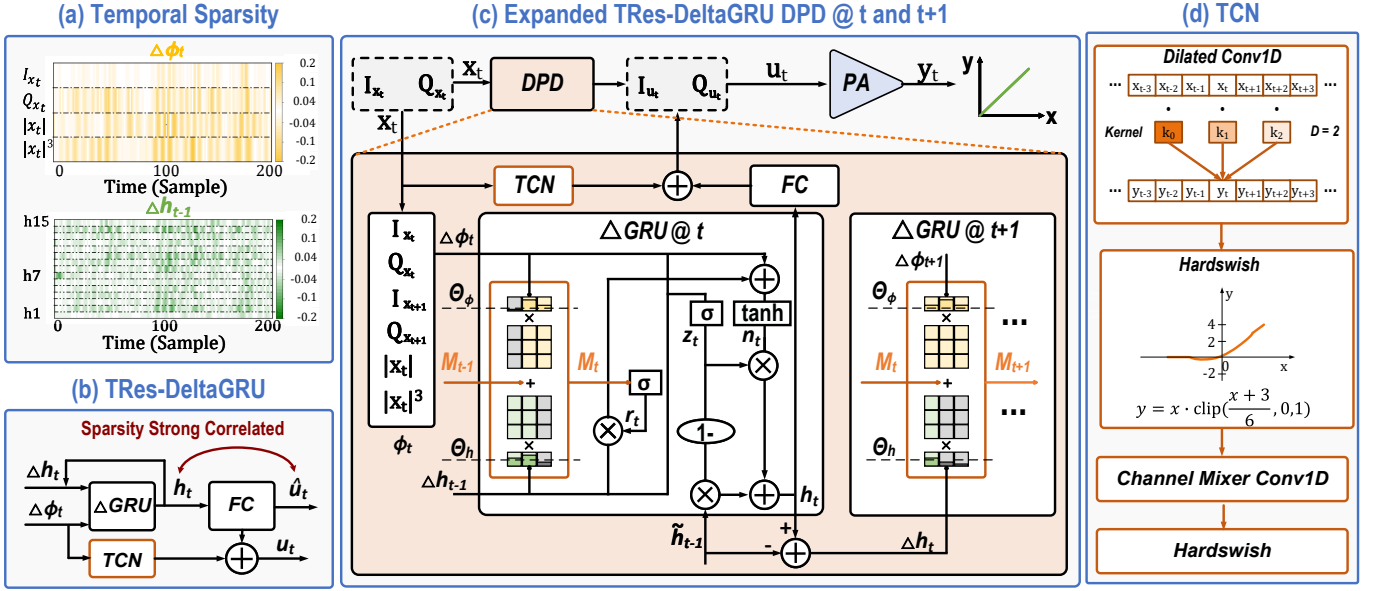


Fig. 3. (a) Temporal sparsity in RNN-based DPD. (b) Schematic of TRes-DeltaGRU. (c) Unfolded TRes-DeltaGRU DPD at t and $t+1$. (d) Layers of TCN Residual Path.

- 2) **Temporally-Sparse DPD Learning (Fig. 2b):** Building upon the DPD learning step of OpenDPDv1, OpenDPDv2 introduces the TRes-DeltaGRU algorithm with Delta threshold mechanisms. The Delta NN-based DPD model employs temporal sparsity through delta thresholds Θ_ϕ and Θ_h to achieve computational efficiency. The Delta DPD model π_{DPD} is cascaded before the pre-trained, frozen π_{PA} , to form the cascaded model π_{CAS} . Using BPTT, π_{CAS} is trained to approximate a linear transfer function with $\mathbf{x}[n]$ as input and $G\mathbf{x}[n]$ as output, enabling π_{DPD} to learn the inverse of the PA behavior.
- 3) **Quantization-Aware Optimization (Fig. 2c):** OpenDPDv2 implements quantization-aware training as the fourth step [26] to optimize the TRes-DeltaGRU DPD model for hardware deployment. During training, full-precision variables are updated during gradient descent while quantized values are used in forward propagation. This methodology reduces computational complexity and enables energy-efficient hardware implementation while maintaining model performance.

A. The TRes-DeltaGRU Algorithm

Besides the learning and optimization architecture, OpenDPDv2 is embedded with a novel high-performance hybrid-NN DPD model, TRes-DeltaGRU, leveraging light-weight temporal convolution residual path and temporal sparsity of GRU.

1) **Dynamic Temporal Sparsity in DPD input signals and hidden neurons:** The delta processing concept emerges from analyzing the temporal characteristics of DPD signals. We present the input feature set $[I_{x_t}, Q_{x_t}, |x_t|, |x_t|^3]$, as an example for the DPD task. When processing continuous sequential signals using NNs, the changes between consecutive

time steps (Δ) in input neurons, denoted as $\Delta\phi$, and hidden state vectors, denoted as Δh , are depicted in Figure 3 (a). The Delta data in Figure 3 (a) are obtained from a 200 MHz OFDM signal and a 15-hidden-neuron vector employed in our proposed GRU-based model for the DPD task. In Figure 3 (a), white pixels indicate Delta values close to zero, suggesting a redundant representation over time. Consequently, the DPD model can exploit this temporal stability in both the $\Delta\phi$ and Δh sequences to transform dense-matrix-dense-vector multiplication $\mathbf{M} \times \mathbf{V}$ into dense-matrix-sparse-vector multiplication ($\mathbf{M} \times \mathbf{SV}$).

2) **Temporal Residual Path:** In the initial version of DeltaDPD, the GRU layer processes the input feature and its memory effect with a recurrent structure. The predicted DPD outputs are generated by a final Fully-Connected (FC) layer:

$$\hat{\mathbf{u}}_t = \mathbf{W}_{\hat{y}} \mathbf{h}_t + \mathbf{b}_{\hat{y}} \quad (7)$$

However, with this output layer, the sparsity of the pre-distorted DPD output $\hat{\mathbf{u}}_t$ directly depends on the sparsity of the hidden state \mathbf{h}_t . For instance, a 52% sparsity in DeltaDPD [14] reduces the average sampling rate of $\hat{\mathbf{u}}_t$ from 983.04 MHz to approximately 471.86 MHz, potentially degrading linearization performance. To address this dependency, we introduce a residual connection between the input and output layers. While a simple FC layer with the current input step as the residual path could suffice, prior studies [4], [27] suggest that incorporating a memory window enhances DPD performance. However, a large memory window increases the FC layer's number of parameters. To mitigate this, we employ a Temporal Convolutional Networks (TCN) as the residual path, balancing efficiency and performance, as detailed in Figure 3 (b).

3) **TRes-DeltaGRU:** To summarize, the schematic of the expanded TRes-DeltaGRU approach over time is illustrated in Fig. 3 (c). TRes-DeltaGRU approach employs Delta thresholds

Θ_ϕ and Θ_h to bypass multiply-accumulate (MAC) operations and memory accesses associated with Δ vector elements below these thresholds, along with their corresponding weight columns. In the GRU block of Fig. 3 (c), all gray elements represent those skipped during processing.

The sequential $\mathbf{M} \times \mathbf{V}$ operation can be converted to a delta operation as follows:

$$\mathbf{y}_t = \mathbf{W}\mathbf{v}_t, \quad (8)$$

$$\mathbf{y}_t = \mathbf{W}\Delta\mathbf{v}_t + \mathbf{y}_{t-1} = \mathbf{W}(\mathbf{v}_t - \mathbf{v}_{t-1}) + \mathbf{y}_{t-1}, \quad (9)$$

where \mathbf{v}_t represents either the Recurrent Neural Network (RNN) input ϕ_t or the hidden state \mathbf{h}_t vector at time t , \mathbf{W} denotes the weight matrices, and \mathbf{y}_{t-1} is the result of the $\mathbf{M} \times \mathbf{V}$ operation from the previous time step $t - 1$. In Eq. 9, the term $\mathbf{W}\Delta\mathbf{v}_t$ transitions to a dense-matrix-sparse-vector multiplication ($\mathbf{M} \times \mathbf{SV}$) when only computations corresponding to $\Delta\mathbf{v}_t$ elements exceeding the threshold are retained, as described by:

$$\Delta\mathbf{v}_t = \begin{cases} \mathbf{v}_t - \tilde{\mathbf{v}}_{t-1}, & |\mathbf{v}_t - \tilde{\mathbf{v}}_{t-1}| > \Theta_v, \\ 0, & |\mathbf{v}_t - \tilde{\mathbf{v}}_{t-1}| \leq \Theta_v, \end{cases} \quad (10)$$

where $\tilde{\mathbf{v}}$ serves as a memory buffer to store the previous state. To mitigate error accumulation over time by tracking only the most recent significant change, each k -th scalar element \tilde{v}^k of the vector $\tilde{\mathbf{v}}$ is updated only when the corresponding Δv^k surpasses the threshold. This updating rule is defined as:

$$\tilde{v}_{t-1}^k = \begin{cases} v_{t-1}^k, & |v_t^k - \tilde{v}_{t-1}^k| > \Theta_v, \\ \tilde{v}_{t-2}^k, & |v_t^k - \tilde{v}_{t-1}^k| \leq \Theta_v, \end{cases} \quad (11)$$

Compared our initial stage work, we replace the $\sin\theta_t, \cos\theta_t$ in DeltaGRU input feature with a small memory window of input. Therefore, the input feature becomes $\phi_t = [I_t, Q_t, I_{t+1}, Q_{t+1}, |x_t|, |x_t|^3]$, leading to DeltaGRU equations in their delta forms as follows Eqs. 12~15:

$$\mathbf{r}_t = \sigma(\mathbf{M}_{r,t}), \quad (12)$$

$$\mathbf{z}_t = \sigma(\mathbf{M}_{z,t}), \quad (13)$$

$$\mathbf{n}_t = \tanh(\mathbf{M}_{n\phi,t} + \mathbf{r}_t \odot \mathbf{M}_{nh,t}), \quad (14)$$

$$\mathbf{h}_t = (1 - \mathbf{z}_t) \odot \mathbf{h}_{t-1} + \mathbf{z}_t \odot \mathbf{n}_t \quad (15)$$

The terms M_r, M_z, M_n are the pre-activation accumulation of DeltaGRU's reset gate r , update gate z and new gate n , initialized by the biases of gates $\mathbf{M}_{r,0} = \mathbf{b}_{ir}$, $\mathbf{M}_{z,0} = \mathbf{b}_{iz}$, $\mathbf{M}_{n\phi,0} = \mathbf{b}_{in}$, $\mathbf{M}_{nh,0} = \mathbf{b}_{hn}$ and defined by:

$$\mathbf{M}_{r,t} = \mathbf{W}_{ir}\Delta\phi_t + \mathbf{W}_{hr}\Delta\mathbf{h}_{t-1} + \mathbf{M}_{r,t-1}, \quad (16)$$

$$\mathbf{M}_{z,t} = \mathbf{W}_{iz}\Delta\phi_t + \mathbf{W}_{hz}\Delta\mathbf{h}_{t-1} + \mathbf{M}_{z,t-1}, \quad (17)$$

$$\mathbf{M}_{n\phi,t} = \mathbf{W}_{in}\Delta\phi_t + \mathbf{M}_{n\phi,t-1}, \quad (18)$$

$$\mathbf{M}_{nh,t} = \mathbf{W}_{hn}\Delta\mathbf{h}_{t-1} + \mathbf{M}_{nh,t-1}, \quad (19)$$

The final output of the DPD module, \mathbf{U} , is expressed as:

$$[\mathbf{I}_u, \mathbf{Q}_u] = \mathbf{U} = \hat{\mathbf{U}} + \text{TCN}(\mathbf{X}) \quad (20)$$

where $\hat{\mathbf{U}} = \{\hat{\mathbf{u}}_t | \hat{\mathbf{u}}_t = \mathbf{W}_{\hat{y}}\mathbf{h}_t + \mathbf{b}_{\hat{y}}, \mathbf{h}_t \in \mathbb{R}^H, n \in 0, \dots, T - 1\}$. H is the hidden size of DeltaGRU.

The core of the TCN is dilated convolutions, which perform convolution on neighboring parameters in the convolutional

kernel at intervals of D , rather than on consecutive time points of the input, as illustrated in Figure 3 (d). This approach expands the receptive field of a Convolutional Neural Network (CNN) with a kernel size of K from K to $(K - 1) \times D + K$ without increasing the parameter count. The TCN residual path is defined as:

$$\text{TCN} = [\text{Dilated Conv1D}, \text{Hardswish}, \text{Conv1D}, \text{Hardswish}] \quad (21)$$

where the Hardswish activation function is:

$$y = x \cdot \text{clip}\left(\frac{x+3}{6}, 0, 1\right) \quad (22)$$

B. Quantization-Aware DPD Learning

[28] and [29] demonstrates that **MAC** operations using 8-bit fixed-point integers (**INT8**) achieve up to $20\times$ greater energy efficiency than **FP32 MAC** operations in 45nm and 7nm technology nodes. Although 32-bit floating-point (**FP32**) arithmetic improves precision, it elevates E_{INF} , reducing energy efficiency. Previous research shows that deep neural networks (DNNs) employing low-precision, fixed-point computations significantly lower memory demands in applications like image recognition and large language models, with negligible accuracy loss. By integrating quantization into TRes-DeltaGRU, our framework further optimizes energy consumption while preserving DPD performance. The gradient of the Round function is approximated using the straight-through estimator [30] to ensure effective training.

The quantization process from floating-point data x to fixed-point representation q is computed as:

$$q = s \times \text{Round}\left(\text{Clip}\left(\frac{x}{s}, Q_{\min}, Q_{\max}\right)\right)$$

where s is the quantization scale, and $[Q_{\min}, Q_{\max}]$ are quantization range, the Clip function restricts the signed input to the range from $Q_{\min} = -2^{n-1}$ to $Q_{\max} = 2^{n-1} - 1$ for n -bit quantization. The Round function rounds the result to the nearest integer. During training, the quantization scale s for each neural network layer is optimized through gradient descent and adjusted to the nearest power-of-two, ensuring the fixed-point representation captures the densely distributed input range.

C. Theoretical Energy Saving

Previous DPD algorithms typically assume a FP32 bit-width for active parameters when evaluating model complexity. However, the number representation format and bit-width of parameters significantly influence energy consumption during hardware implementation. For NNs, the forward pass energy consumption E_F can be expressed as:

$$E_F = E_{\text{MUL}} + E_{\text{ADD}} + E_{\text{MEM}} \quad (23)$$

where E_{MUL} , E_{ADD} , and E_{MEM} are the total energy consumption of all multiplications (**MUL**), additions (**ADD**), and memory accesses (**MEM**) during a forward pass, respectively. When mapping from floating-point to fixed-point parameters with identical bit-width, the energy of arithmetic

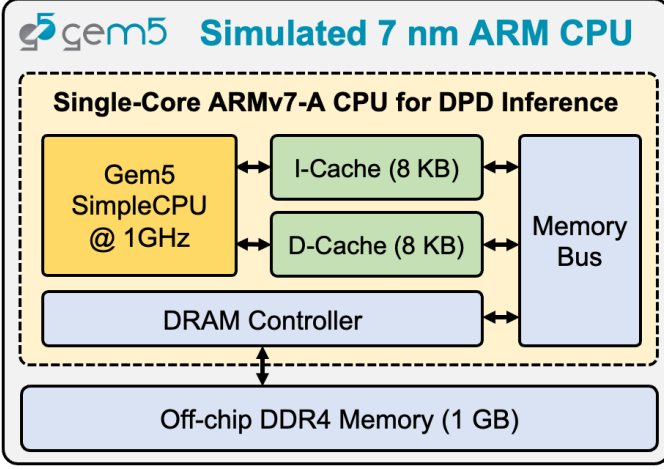


Fig. 4. Microarchitecture of the Gem5-simulated single-core CPU with the 32-bit ARMv7-A instruction set for DPD inference energy estimation under the 7 nm technology.

operations and memory access is reduced due to simpler fixed-point arithmetic hardware. For quantized fixed-point models, we define α as the ratio between lower bit widths and 32 bits ($\alpha = 0.5$ for INT16 vs. INT32). Incorporating both quantization and temporal sparsity percentage Γ , the operation and memory access energy numbers are given by:

$$E_{\text{MUL}} = (1 - \Gamma) \cdot \alpha^2 \cdot E_{\text{MUL,INT32}} \quad (24)$$

$$E_{\text{ADD}} = (1 - \Gamma) \cdot \alpha \cdot E_{\text{ADD,INT32}} \quad (25)$$

$$E_{\text{MEM}} = (1 - \Gamma) \cdot \alpha \cdot E_{\text{MEM,INT32}} \quad (26)$$

D. Hardware Architecture for Energy Simulation

To provide accurate energy consumption estimates that reflect real-world Von Neumann architecture-based processors, this work employs the timing-accurate Gem5 [31] processor microarchitecture simulator to provide detailed statistics on instruction execution, memory hierarchy behavior, and system-level performance metrics.

1) *Simulated Microarchitecture*: The simulated processor implements a 32-bit ARM architecture targeting embedded computing scenarios suitable for DPD deployment. Fig. 4 illustrates the complete microarchitecture, featuring:

- An ARM Timing Simple **CPU core** using the ARMv7-A Instruction Set Architecture (ISA) with Thumb support.
- A **cache hierarchy** consists of separate L1 instruction (I-cache) and data caches (D-cache), each configured as 8KB, 4-way set-associative structures with 64-byte cache lines. We omit L2 and L3 caches to model resource-constrained embedded processors typical in the digital back-end modules in RF systems.
- A main DDR4 memory of 1GB connected to the CPU through the memory bus.

2) *Energy Modeling Framework*: The energy consumption analysis leverages detailed operation counts and memory access patterns extracted from Gem5 simulations, combined with energy characteristics of 7nm CMOS technology [29].

Energy consumption for arithmetic operations varies across data types. For FP32 operations, addition consumes 0.38 pJ

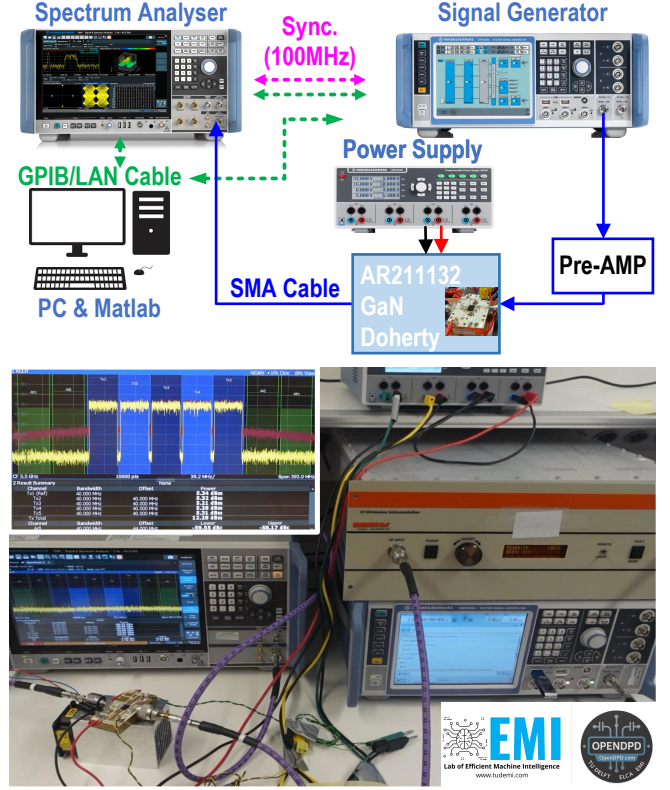


Fig. 5. Setup for dataset acquisition and DPD performance measurement.

while multiplication requires 1.31 pJ per operation. Integer operations exhibit quadratic scaling for multiplication and linear scaling for addition relative to bit-width. Specifically, INT16 operations consume approximately 0.015 pJ (addition) and 0.37 pJ (multiplication), while INT12 operations require 0.011 pJ (addition) and 0.21 pJ (multiplication).

Memory hierarchy energy consumption scales with both access frequency and data width. L1 cache accesses consume 7.5 pJ per access, while the DDR4 memory accesses require 1.3 nJ per transfer. The energy model incorporates data-width scaling factors: FP32 (1.0 \times), INT16 (0.5 \times), and INT12 (0.375 \times) to account for reduced data movement in quantized implementations.

IV. EXPERIMENTAL SETUP

A. Measurement Setup

Figure 5 depicts the experimental setup utilized in this study. The OFDM baseband I/Q signal was generated by an R&S-SMW200A signal generator and amplified by a PA with the same average output power, with and without DPD. The resulting output signal was digitized using an R&S-FSW43 spectrum analyzer. During the ACPR measurements, the resolution bandwidth is set as 100 Hz to decrease the noise floor of the spectrum analyzer [32]. The EVM was computed by comparing the input signal with the digitized output signal instead of the reference grid.

B. Test Signals and Design-Under-Test (DUT)

The experiment employed APA_200MHz, a TM3.1a 5×40 -MHz (200-MHz) 256-QAM signal with a Peak-to-Average Power Ratio (PAPR) of 10.0dB and sampling rate of 983.04MHz. The dataset, consisting of 98304 samples, was split into 60% for training, 20% for validation, and 20% for testing. Additionally, the experiments were conducted on a 3.5GHz GaN Doherty PA DUT, operating at an average output power of 41.5dBm.

C. Neural Network Training

The end-to-end training process was implemented using OpenDPDv2 platform. Models were trained offline for 240 epochs using the ADAMW optimizer, configured with an initial learning rate of $5E-3$, a ReduceOnPlateau decay strategy, and a batch size of 64. In the model comparison experiment, the Decomposed Vector Rotation (DVR) decomposition included 3 units, the Phase Gated (PG)-Just Another NETwork (JANET) model utilized a window size of 4. Both JANET models had a hidden size of 12, while the TRes-DeltaGRU model utilized 15 hidden neurons. For the temporal residual layer, the Conv1D hyperparameters are defined as (C_{in}, C_{out}, K, D) , where C_{in} and C_{out} represent the input and output channel sizes, respectively, K is the kernel size, D is the dilation length, and P is the padding size. Non-causal convolution was applied with a padding size of D . The hyperparameters for the first dilated convolutional layer were set to $(2, 3, 3, 16)$, and for the channel mixer, they were $(3, 2, 1, 0)$. The stride of the Conv1D layer was consistently set to 1.

All experiments were performed on a single NVIDIA RTX 4090 GPU running PyTorch version 2.4.1 with CUDA version 12.4. During DPD learning, models achieving the best ACPR were saved for final evaluation.

D. Gem5 Simulation Setup

The simulation begins with cross-compilation of DPD algorithms in C programs targeting the ARMv7-A ISA. Program binaries are generated using the arm-linux-gnueabi-hf-gcc cross-compiler with optimization flags `-O3 -march=armv7-a -mcpu=neon -static` to maximum compilation optimization and make use of the NEON single-instruction-multiple-data (SIMD) vector processing unit.

During simulation, Gem5 loads the target binary into the simulated DDR4 memory and executes the DPD algorithms with an I/Q sequence length of 10,000.

V. RESULTS AND DISCUSSIONS

We evaluate the absolute linearization performance of OpenDPDv2-trained TRes-DeltaGRU DPD models of various levels of complexity versus prior works. For giving an intuitive measure of the sparse DPD model complexity and simplified comparison, we define the number of active parameters of TRes-DeltaGRU as:

$$\begin{aligned} \# \text{Active Params} = & \# \text{DeltaGRU Params} \times (1 - \Gamma) \\ & + \# \text{FC Params} + \# \text{TCN Params} \end{aligned} \quad (27)$$

TABLE I
LINEARIZATION PERFORMANCE OF 15-HIDDEN NEURON TRES-GRU VS. TRES-DELTA GRU MODELS EVALUATED WITH TM3.1A 200-MHZ 5-CHANNEL \times 40-MHZ 256-QAM OFDM SIGNALS SAMPLED AT 983.04 MHZ ALONGSIDE THEIR ESTIMATED DYNAMIC POWER CONSUMPTION

DPD Model		Temporal Sparsity	#Active Params	Model Precision	ACPR (dBc)	EVM (dB)
OpenDPDv1						
Without DPD		-	-	-	-26.3	-22.3
RVTDCNN [33]		-	1007	-	-51.8	-32.4
PG-JANET [2]		-	1130	FP32	-52.9	-39.9
DVR-JANET [3]		-	1097	-	-53.8	-38.2
OpenDPDv2						
Without DPD		-	-	-	-28.6	-22.7
Dense Model	DGRU [12]	-	1041	-	-58.4	-39.1
	TRes	-	999	FP32	-59.1	-41.7
	-	-	524	-	-52.7	-37.3
	GRU	-	311	-	-52.3	-34.1
Delta Model	TRes - DeltaGRU	0%	996	FP32	-59.4	-42.1
				W16A16	-58.8	-41.2
				W12A12	-54.5	-37.3
		56.0%	450	FP32	-52.9	-35.7
				W16A16	-53.2	-39.3
				W12A12	-50.3	-35.2
		72.5%	288	FP32	-52.0	-37.0
				W16A16	-48.2	-34.2
				W12A12	-46.9	-31.0

Table I compares ACPR and EVM results for the TRes-DeltaGRU model across various temporal sparsity and precision levels, alongside counts of operations and memory access. Notably, the W16A16 TRes-DeltaGRU-450 model surpasses the FP32 TRes-GRU-524 model by 0.5dB in ACPR and 2dB in EVM. Here, the 450 and 524 refer to the number of active parameters of the corresponding models. Similarly, the FP32 TRes-DeltaGRU-288 with fewer active parameters outperforms the TRes-GRU-311 model in linearization performance. These results validate the efficacy of DeltaDPD methods in achieving better linearization with reduced energy consumption. Additionally, the W12A12 TRes-DeltaGRU-288 DPD model meets 3GPP spectrum mask of -45dBc and EVM standards of -30dB with the lowest energy cost, attaining an ACPR of -46.9dBc and an EVM of -31.0dB.

A. Delta Threshold Scan

A Delta threshold scan was conducted on a 15-hidden-neuron TRes-DeltaGRU model with varying thresholds Θ_ϕ from 0 to 0.04 and Θ_h from 0 to 0.4. Figures 6 (a) and (b) depict the average ACPR and EVM of FP32 TRes-DeltaGRU models, while (c) illustrates the number of activated parameters. Fig. 6 (d) reflects the influence of GRU temporal sparsity on linearization performance. The TRes-DeltaGRU-996 model achieves an average ACPR of -59.4dBc and an EVM of -42.1dB, surpassing the DeltaGRU-1067 model by 5.1dBc in ACPR [14]. This improvement confirms that the TCN residual path enhances DPD model performance. Furthermore, the TRes-DeltaGRU-450 model with $\Theta_\phi = 0.01$ and $\Theta_h = 0.05$ achieves an ACPR 2.9dB higher than the DeltaGRU-573 model with $\Theta_\phi = 0.0$ and $\Theta_h = 0.05$. These results

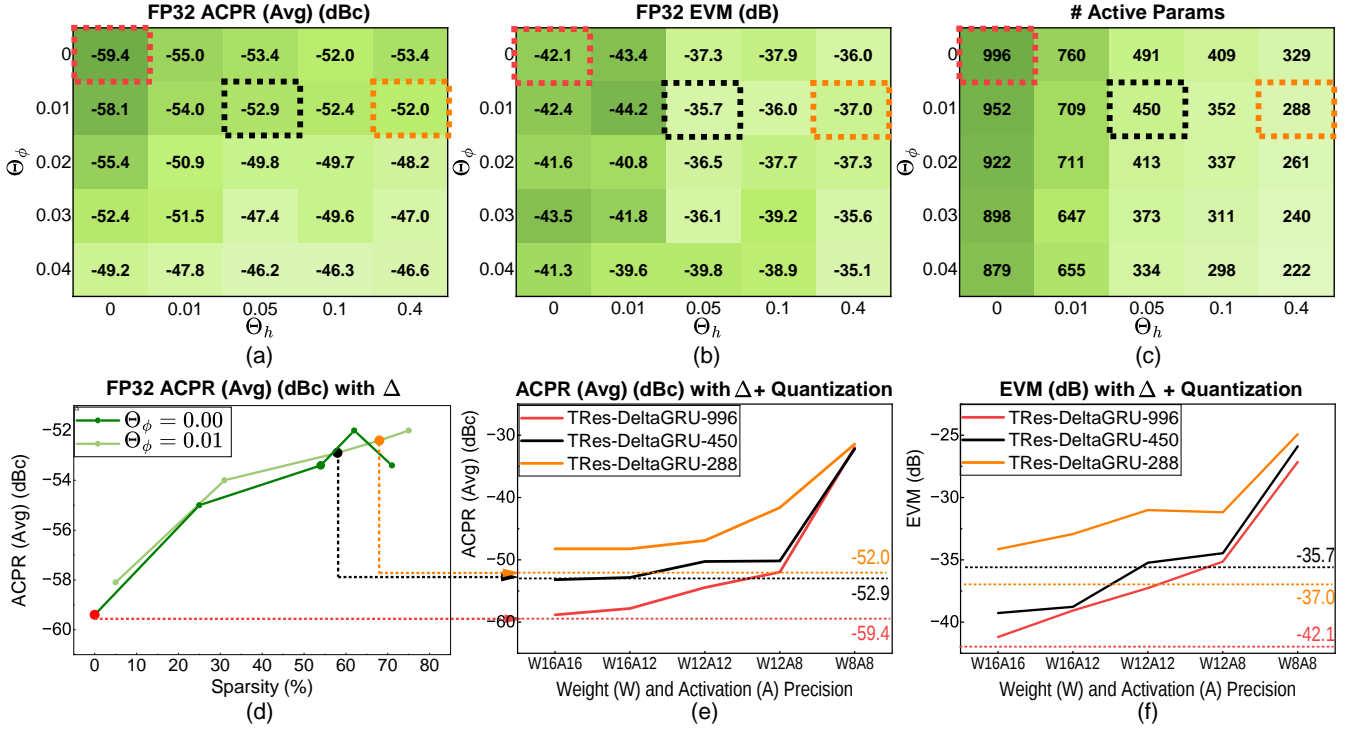


Fig. 6. Delta Threshold scan of TRes-DeltaGRU vs. (a) Average ACPR (dBc) (b) EVM (dB) (c) Number of active parameters; (d) Average ACPR (dBc) vs. sparsity with only delta. Quantization precision scan vs. (e) Average ACPR (dBc) (f) EVM (dB)

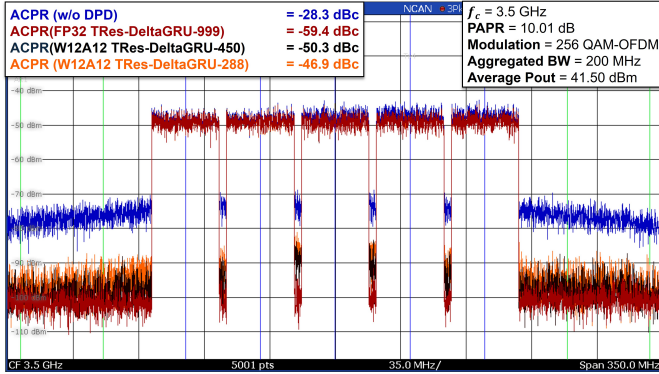


Fig. 7. Measured spectrum on the 200 MHz TM3.1a signal without DPD and with TRes-DeltaGRU DPD.

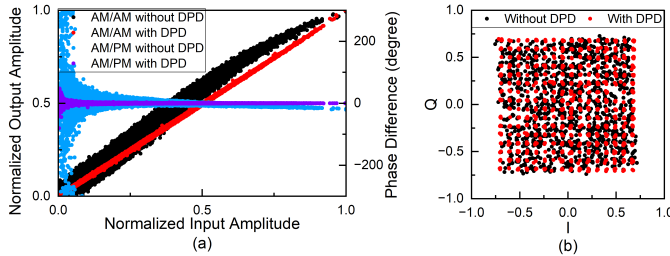


Fig. 8. (a) AM/AM and AM/PM characteristic (b) constellation on the 200 MHz TM3.1a signal without DPD and with FP32 TRes-DeltaGRU-996 DPD.

demonstrate that the TCN residual path decouples the DPD output sampling rate from Δh , enabling greater sparsity and improved linearization. At higher thresholds ($\Theta_\phi = 0.04$, $\Theta_h = 0.4$), the number of activated parameters decreases to 222, with the FP32 TRes-DeltaGRU-222 model achieving 80.2% temporal sparsity, yielding an ACPR of -46.7 dBc and an EVM of -35.1 dB, reflecting a trade-off between sparsity and performance.

B. Model Precision Scan

Figures 6 (e) and (f) illustrate the relationship between weight and activation precision and ACPR/EVM for the TRes-DeltaGRU DPD model with parameter counts of approximately 300, 450, and 1000. The TRes-DeltaGRU-450 model maintains an ACPR better than -45 dBc until model precision is reduced to W12A8. The trend of results shows that reduced power consumption can be attained by adopting lower precision, though this compromises accuracy.

Figs. 7 depicts the measured spectrum of various quantized TRes-DeltaGRU models. Fig. 8 (a) shows the AM/AM and AM/PM characteristics, and (b) shows the constellation without DPD and with FP32 TRes-DeltaGRU-996 model.

C. Energy Analysis

This section evaluates the energy efficiency of the TRes-DeltaGRU algorithm under varying quantization precisions and temporal sparsity levels. Accurate energy estimations are provided using the Gem5-simulated ARM CPU to deliver insights critical for practical, energy-constrained RF systems. DDR4 memory energy is excluded from the

analysis, as it is only utilized during initialization, and the 8KB D-cache sufficiently accommodates the entire DPD model, reflected by nearly 100% L1 cache hit rates.

Figure 9 demonstrates how forward pass energy consumption (E_F) decreases as temporal sparsity increases in the TRes-DeltaGRU-996 DPD model. With INT12 quantization alone (no temporal sparsity), the energy is reduced by $2.8\times$ compared to FP32 implementations, maintaining an ACPR of -54.5 dBc. When combined with a temporal sparsity of 72.5%, this model achieves an energy reduction factor of $5.2\times$, while still adhering to a common ACPR specification over -45 dBc. These results confirm OpenDPDv2’s effectiveness in significantly decreasing energy demands without compromising critical linearization performance.

Figure 10 provides a breakdown of forward pass energy consumption for the TRes-DeltaGRU-996 DPD model operating at INT16 precision across different sparsity levels. A key insight is that memory access dominates overall energy consumption as D-cache energy alone surpasses arithmetic operation energy by more than an order of magnitude. Consequently, future hardware implementations should prioritize reducing memory access through joint algorithmic and circuit-level optimizations, emphasizing algorithm-hardware co-design [34]. Furthermore, Figure 10 also reveals that increased temporal sparsity leads to a higher relative proportion of I-cache energy consumption, attributed to overhead operations such as delta vector encoding, memory updates, and indexing. While this overhead can diminish the benefits of sparsity in general-purpose CPUs, a specialized ASIC implementation can effectively mitigate these inefficiencies, further enhancing energy savings.

The absolute energy numbers evaluated by Gem5 are overall significantly larger than the rough estimation reported in [13], [14], which is because prior works assumed 100% reuse of operands in an ideal multiply-and-accumulate array without overhead. In contrast, our Gem5-based analysis incorporates realistic processor behaviors and overheads associated with general-purpose 32-bit instruction set architectures. Therefore, the sum of arithmetic and D-cache energy values will provide a more accurate benchmark for potential ASIC implementations.

VI. CONCLUSION

This paper introduces the OpenDPDv2 framework, aiming to streamline DPD model learning, optimization, and standard datasets for better simulation. The OpenDPDv2 framework is packed with a new DPD model, TRes-DeltaGRU, leveraging quantization and temporal sparsity. Results show proposed FP32 TRes-DeltaGRU-996 achieves the state-of-the-art linearization performance with 200 MHz OFDM signal. By reducing computational complexity and memory access compared to conventional approaches, quantized TRes-DeltaGRU achieves a saving of E_F , which helps to bring down the both inference and online adaptation energy consumption of NN DPDs, while maintaining robust linearization performance.

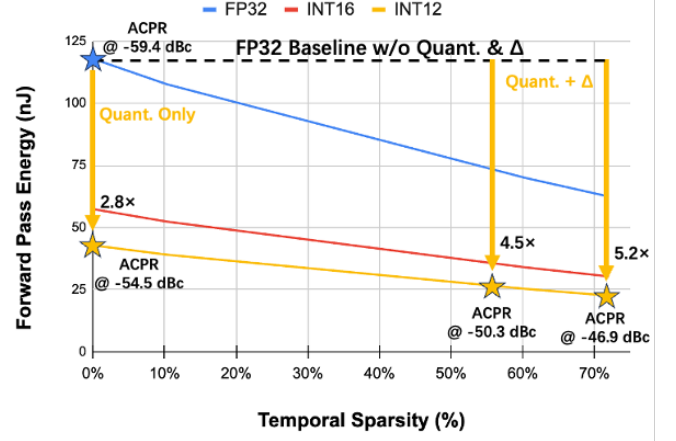


Fig. 9. TRes-DeltaGRU-996 DPD forward pass energy (E_F) reduction with temporal sparsity estimated using the Gem5-simulated ARM CPU.

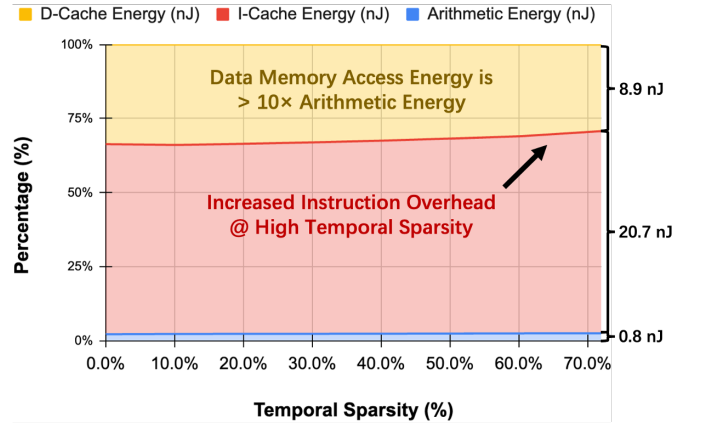


Fig. 10. TRes-DeltaGRU-996 (INT16) DPD forward pass energy breakdown on the Gem5-simulated ARM CPU.

ACKNOWLEDGMENT

We thank Yi Zhu and John Gajadharsing from Ampleon for lending us the PA DUT and assistance in building the experimental setup. We also thank Prof. Leo C. N. de Vreede from Delft University of Technology and Prof. Anding Zhu from University College Dublin for related technical discussions and writing suggestions. This work is partially supported by the European Research Executive Agency (REA) under the Marie Skłodowska-Curie Actions (MSCA) Postdoctoral Fellowship program, Grant No. 101107534 (AIRHAR).

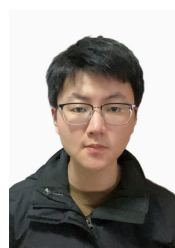
REFERENCES

- [1] “3gpp specification series,” Available at <https://www.3gpp.org/dynareport?code=38-series.htm>.
- [2] T. Kobal, Y. Li, X. Wang, and A. Zhu, “Digital predistortion of RF power amplifiers with phase-gated recurrent neural networks,” *IEEE Trans. Microw. Theory Techn.*, vol. 70, no. 6, p. 3291–3299, Jun 2022.
- [3] T. Kobal and A. Zhu, “Digital predistortion of RF power amplifiers with decomposed vector rotation-based recurrent neural networks,” *IEEE Trans. Microw. Theory Techn.*, vol. 70, no. 11, p. 4900–4909, Nov 2022.
- [4] A. Fischer-Bühner, L. Anttila, M. Dev Gomony, and M. Valkama, “Recursive neural network with phase-normalization for modeling and linearization of rf power amplifiers,” *IEEE Microwave and Wireless Technology Letters*, vol. 34, no. 6, pp. 809–812, 2024.

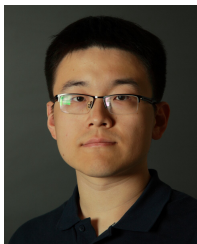
- [5] Q. Zhang, C. Jiang, G. Yang, R. Han, and F. Liu, "Block-oriented recurrent neural network for digital predistortion of rf power amplifiers," *IEEE Transactions on Microwave Theory and Techniques*, vol. 72, no. 7, pp. 3875–3885, 2024.
- [6] S. Wesemann, J. Du, and H. Viswanathan, "Energy efficient extreme mimo: Design goals and directions," *IEEE Communications Magazine*, vol. 61, no. 10, pp. 132–138, 2023.
- [7] Y. Li, X. Wang, and A. Zhu, "Sampling rate reduction for digital predistortion of broadband RF power amplifiers," *IEEE Trans. Microw. Theory Tech.*, vol. 68, no. 3, pp. 1054–1064, 2020.
- [8] N. Hammler, A. Cathelin, P. Cathelin, and B. Murmann, "A spectrum-sensing dpd feedback receiver with $30\times$ reduction in adc acquisition bandwidth and sample rate," *IEEE Transactions on Circuits and Systems I: Regular Papers*, vol. 66, no. 9, pp. 3340–3351, 2019.
- [9] Y. Li, X. Wang, and A. Zhu, "Reducing power consumption of digital predistortion for RF power amplifiers using real-time model switching," *IEEE Trans. Microw. Theory Tech.*, vol. 70, no. 3, pp. 1500–1508, 2022.
- [10] M. Beikmirza, L. C. de Vreede, and M. S. Alavi, "A low-complexity digital predistortion technique for digital i/q transmitters," in *2023 IEEE/MTT-S International Microwave Symposium - IMS 2023*, 2023, pp. 787–790.
- [11] Z. Liu, X. Hu, L. Xu, W. Wang, and F. M. Ghannouchi, "Low computational complexity digital predistortion based on convolutional neural network for wideband power amplifiers," *IEEE Transactions on Circuits and Systems II: Express Briefs*, vol. 69, no. 3, pp. 1702–1706, 2022.
- [12] Y. Wu, G. D. Singh, M. Beikmirza, L. C. N. de Vreede, M. Alavi, and C. Gao, "OpenDPD: An Open-Source End-to-End Learning & Benchmarking Framework for Wideband Power Amplifier Modeling and Digital Pre-Distortion," *arXiv preprint arXiv:2401.08318*, 2024.
- [13] Y. Wu, A. Li, M. Beikmirza, G. D. Singh, Q. Chen, L. C. N. de Vreede, M. Alavi, and C. Gao, "Mp-dpd: Low-complexity mixed-precision neural networks for energy-efficient digital predistortion of wideband power amplifiers," *IEEE Microwave and Wireless Technology Letters*, pp. 1–4, 2024.
- [14] Y. Wu, Y. Zhu, K. Qian, Q. Chen, A. Zhu, J. Gadajarsing, L. C. N. de Vreede, and C. Gao, "Deltadpd: Exploiting dynamic temporal sparsity in recurrent neural networks for energy-efficient wideband digital predistortion," *IEEE Microwave and Wireless Technology Letters*, pp. 1–4, 2025.
- [15] H. Duan, M. Versluis, Q. Chen, L. C. N. de Vreede, and C. Gao, "Tcn-dpd: Parameter-efficient temporal convolutional networks for wideband digital predistortion," 2025. [Online]. Available: <https://arxiv.org/abs/2506.12165>
- [16] A. Paszke, S. Gross, F. Massa, A. Lerer, J. Bradbury, G. Chanan, T. Killeen, Z. Lin, N. Gimelshein, L. Antiga, A. Desmaison, A. Kopf, E. Yang, Z. DeVito, M. Raison, A. Tejani, S. Chilamkurthy, B. Steiner, L. Fang, J. Bai, and S. Chintala, "Pytorch: An imperative style, high-performance deep learning library," in *Adv. Neural Inf. Process. Syst.*, H. Wallach, H. Larochelle, A. Beygelzimer, F. d'Alché-Buc, E. Fox, and R. Garnett, Eds., vol. 32. Curran Associates, Inc., 2019. [Online]. Available: https://proceedings.neurips.cc/paper_files/paper/2019/file/bdbca288fec7f92f2bfa9f7012727740-Paper.pdf
- [17] N. Hammler, A. Cathelin, P. Cathelin, and B. Murmann, "A spectrum-sensing dpd feedback receiver with $30\times$ reduction in adc acquisition bandwidth and sample rate," *IEEE Transactions on Circuits and Systems I: Regular Papers*, vol. 66, no. 9, pp. 3340–3351, 2019.
- [18] A. Fischer-Bühner, L. Anttila, A. Brihuega, M. Dev Gomony, and M. Valkama, "Predistortion of gan power amplifier transient responses in time-division duplex using machine learning," *IEEE Microwave and Wireless Technology Letters*, vol. 35, no. 6, pp. 924–927, 2025.
- [19] D. E. Rumelhart, G. E. Hinton, and R. J. Williams, "Learning representations by back-propagating errors," *nature*, vol. 323, no. 6088, pp. 533–536, 1986.
- [20] Texas Instruments, "ADC12SJ1600 12-Bit, 1.6-GSPS, RF-Sampling Analog-to-Digital Converter (ADC)," https://www.ti.com/lit/ds/symlink/adc12sj1600.pdf?ts=1751638711567&ref_url=https%253A%252F%252Fwww.ti.com%252Fdata-convertisers%252Fadc-circuit%252Fproducts.html, May 2025, accessed: Jul. 4, 2025.
- [21] Y. Li, X. Wang, and A. Zhu, "Complexity-reduced model adaptation for digital predistortion of rf power amplifiers with pretraining-based feature extraction," *IEEE Transactions on Microwave Theory and Techniques*, vol. 69, no. 3, pp. 1780–1790, 2021.
- [22] W. Li, R. Criado, W. Thompson, K. Chuang, G. Montoro, and P. L. Gilabert, "Gpu-based implementation of pruned artificial neural networks for digital predistortion linearization of wideband power amplifiers," *Authorea Preprints*, 2024.
- [23] M. Versluis, Y. Wu, and C. Gao, "Sparsedpd: A sparse neural network-based digital predistortion fpga accelerator for rf power amplifier linearization," 2025. [Online]. Available: <https://arxiv.org/abs/2506.16591>
- [24] A. Li, H. Wu, Y. Wu, Q. Chen, L. C. N. de Vreede, and C. Gao, "Dpd-neuralengine: A 22-nm 6.6-tops/w/mm² recurrent neural network accelerator for wideband power amplifier digital pre-distortion," in *2025 IEEE International Symposium on Circuits and Systems (ISCAS)*, 2025, pp. 1–5.
- [25] N. Hammler, *Sub-Nyquist Receiver for Digital Predistortion of RF Power Amplifiers*. Stanford University, 2019.
- [26] M. Nagel, M. Fournarakis, R. A. Amjad, Y. Bondarenko, M. van Baalen, and T. Blankevoort, "A white paper on neural network quantization," *CoRR*, vol. abs/2106.08295, 2021. [Online]. Available: <https://arxiv.org/abs/2106.08295>
- [27] D. Wang, M. Aziz, M. Helou, and F. M. Ghannouchi, "Augmented real-valued time-delay neural network for compensation of distortions and impairments in wireless transmitters," *IEEE Trans. Neural Netw. Learn. Syst.*, vol. 30, no. 1, pp. 242–254, Jan 2019.
- [28] M. Horowitz, "1.1 computing's energy problem (and what we can do about it)," in *2014 IEEE international solid-state circuits conference digest of technical papers (ISSCC)*. IEEE, 2014, pp. 10–14.
- [29] N. P. Jouppi, D. H. Yoon, M. Ashcraft, M. Gottscho, T. B. Jablin, and K. G. et al, "Ten lessons from three generations shaped google's TPuv4i: Industrial product," in *2021 ACM/IEEE 48th Annual International Symposium on Computer Architecture (ISCA)*. IEEE, 2021, pp. 1–14.
- [30] Y. Bengio, N. Léonard, and A. Courville, "Estimating or propagating gradients through stochastic neurons for conditional computation," *arXiv preprint arXiv:1308.3432*, 2013.
- [31] J. Lowe-Power, A. M. Ahmad, A. Akram, M. Alian, R. Amslinger, M. Andreozzi et al., "The gem5 simulator: Version 20.0+," 2020. [Online]. Available: <https://arxiv.org/abs/2007.03152>
- [32] Texas Instruments, "Understanding basic spectrum analyzer operation," https://www.rohde-schwarz.com/us/products/test-and-measurement/essentials-test-equipment/spectrum-analyzers/understanding-basic-spectrum-analyzer-operation_256005.html, May 2025, accessed: Jul. 4, 2025.
- [33] X. Hu, Z. Liu, X. Yu, Y. Zhao, W. Chen, and B. e. a. Hu, "Convolutional neural network for behavioral modeling and predistortion of wideband power amplifiers," *IEEE Transactions on Neural Networks and Learning Systems*, vol. 33, no. 8, pp. 3923–3937, 2022.
- [34] S.-C. Liu, C. Gao, K. Kim, and T. Delbruck, "Energy-efficient activity-driven computing architectures for edge intelligence," in *2022 International Electron Devices Meeting (IEDM)*, 2022, pp. 21.2.1–21.2.4.



Yizhuo Wu (Graduate Student Member, IEEE) obtained her M.Sc. degree in Microelectronics at TU Delft in 2023. She is now a PhD student supervised by Dr. Chang Gao in the Lab of Efficient Circuits & systems for Machine Intelligence (EMI). Her research focuses on software-hardware co-designed AI for I/Q signal processing, which aims to find energy-efficient solutions for high-frequency signal processing tasks.



Ang Li (Graduate Student Member, IEEE) received the B.S. degree in Microelectronics from the School of Microelectronics, Xidian University, Xi'an, China, in 2019, and the M.S. degree in Integrated Circuits from the School of Integrated Circuits, Tsinghua University, Beijing, China, in 2022. He is currently pursuing a Ph.D. in the Department of Microelectronics at Delft University of Technology, The Netherlands. His research interests include deep learning, digital circuit design, computer vision, and VLSI digital signal processing.



Chang Gao (Member, IEEE) received his Ph.D. degree with Distinction in Neuroscience from the Institute of Neuroinformatics, University of Zürich and ETH Zürich, Zürich, Switzerland, in March 2022 and his master degree from Imperial College London in September 2016 and his bachelor degree from University of Liverpool and Xi'an Jiaotong-Liverpool University in July 2015. Since August 2022, he has been an assistant professor in the Department of Microelectronics at TU Delft, The Netherlands, where he leads the Lab of Efficient

Machine Intelligence (EMI), focusing on neuromorphic algorithm-hardware co-design for edge AI computing. He received the 2022 Misha Mahowald Early Career Award in Neuromorphic Engineering and the 2022 Marie-Curie Postdoctoral Fellowship. He is a 2023 Dutch Research Council (NWO) Veni laureate and a 2023 MIT Technology Review Innovator Under 35 in Europe for his contribution to algorithm-hardware co-design for efficient sparse recurrent neural network edge computing.